RESEARCH ARTICLE

Volcanic jets, plumes, and collapsing fountains: evidence from large-scale experiments, with particular emphasis on the entrainment rate

**P. Dellino · F. Dioguardi · D. Mele · M. D'Addabbo ·
B. Zimanowski · R. Büttner · D. M. Doronzo · I. Sonder ·
R. Sulpizio · T. Dürig · L. La Volpe**

Abstract The source conditions of volcanic plumes and collapsing fountains are investigated by means of large-scale experiments. In the experiments, gas-particle jets issuing from a cylindrical conduit are forced into the atmosphere at different mass flow rates. Dense jets (high particle volumetric concentration, e.g., $C_0 > 0.01$) generate collapsing fountains, whose height scales with the squared exit velocity. This is consistent with Bernoulli's equation, which is a good approximation if air entrainment is negligible. In this case, kinetic energy is transformed into potential energy without any significant loss by friction with the atmosphere. The dense collapsing fountain, on hitting the ground, generates an intense shear flow similar to a pyroclastic density current. Dilute hot jets (low particle volumetric concentration, e.g., $C_0 < 0.01$) dissipate their initial kinetic energy at much smaller heights than those predicted by Bernoulli's equation. This is an indication that part of the total mechanical energy is lost by friction with the atmosphere. Significant air entrainment results in this case, leading to the formation of a buoyant column (plume) from which particles settle similarly to pyroclastic fallout. The direct measurement of entrainment coefficient in the experiments suggests that dense collapsing fountains form only when air entrainment is not significant. This is a consequence of the large density difference between the jet and the atmosphere. Cold dilute experiments result in an entrainment coefficient of about 0.06, which is typical of pure jets of fluid dynamics. Hot dilute experiments result in an entrainment coefficient of about 0.11, which is typical of thermally buoyant plumes. The entrainment coefficients obtained by experiments were used as input data in numerical simulations of fountains and plumes. A numerical model was used to solve the classic top-hat system of governing equations, which averages the field variables (e.g., column velocity and density) across the column. The maximum heights calculated with the model agree well with those observed experimentally, showing that our entrainment coefficients are compatible with a top-hat model. Dimensional analysis of the experimental data shows that a value of 3 for the source densimetric Froude number characterizes the transition between dense collapsing fountains and dilute plumes. This value delimits the source conditions (exit velocity, conduit radius, and particle volumetric concentration) for pyroclastic flow (<3) and fallout (>3).

Editorial responsibility: S. A. Fagents

P. Dellino · F. Dioguardi (✉) · D. Mele · M. D'Addabbo ·
D. M. Doronzo · R. Sulpizio · L. La Volpe
Dipartimento di Scienze della Terra e Geoambientali, Università degli Studi di Bari "Aldo Moro", Bari, Italy
e-mail: fabio.dioguardi@uniba.it

B. Zimanowski · R. Büttner
Physikalisch Vulkanologisches Labor, Universität Würzburg,
Würzburg, Germany

I. Sonder
Center for GeoHazards Studies, University at Buffalo, Buffalo, USA

T. Dürig
Institute of Earth Sciences, University of Iceland, Reykjavík, Iceland

R. Sulpizio
IDPA-CNR, via Mario Bianco 9, Milan, Italy

Introduction

In explosive volcanic eruptions, a gas-particle jet issues at high velocity from the vent and forms an eruption column

that can reach a height of several kilometers. Depending on vent diameter, mass flow rate, particle volumetric concentration, and temperature, the column can collapse and form pyroclastic density currents, or can become buoyant and spread into the atmosphere, from where particles settle to the ground and form pyroclastic fall deposits. The dynamics of volcanic columns are fundamental for hazard assessment, and various models have been developed in the past decades, which are aimed at both constraining the eruptive regime parameters (Wilson et al. 1980; Woods 1988, 2010; Woods and Caulfield 1992; Dellino et al. 2010; Suzuki and Koyaguchi 2012) and modeling pyroclast dispersion (Costa et al. 2006; Sulpizio et al. 2012) and deposition (Woods 1988, 2010).

Given the apparent analogy of the volcanic process with flows issuing from a circular nozzle, fluid dynamics theory describing jets and plumes has been used over the years as a reference to develop models of eruptive columns (Woods 1988, 2010; Formenti et al. 2003; Carazzo et al. 2008).

In fluid dynamics, a pure jet is a fully turbulent flow issuing from a source with a density equal to that of the surrounding environment, and its ascent is driven by initial momentum. A pure plume is a flow that is driven solely by the initial buoyancy, which results from the density difference between the source and the environment (Morton et al. 1956). A buoyant jet is a flow in which both the initial momentum and buoyancy play a role (Papanicolaou and List 1988), whereas a negatively buoyant jet is a flow in which the source fluid has a greater density than the surrounding (Turner 1966, 1986; Papanicolaou et al. 2008). Negatively buoyant jets reach a maximum height then "collapse" and form a fountain (McDougall 1981; Bloomfield and Kerr 2000; Carazzo et al. 2006, 2008, 2010).

The gas-particle flow issuing from a volcanic vent, because of the high density of pyroclastic particles, invariably starts as a negatively buoyant jet. During ascent, it can become buoyant because of air entrainment and heating that cause a significant decrease in the gas-particle mixture density. A convective buoyant column is thus formed, from which particles settle by simple fallout. The large-scale end member of this phenomenon is known as a Plinian column. In contrast, when air entrainment is insufficient, the jet remains denser than the environment, and the flow collapses to form a pyroclastic density current.

Notwithstanding the large variability of eruptive conditions and regimes of explosive phenomena, which encompass both dense and dilute columns, modeling of volcanic columns (Wilson 1976; Wilson et al. 1980; Woods 1988) was based, in the past, on Morton's theory of dilute plumes (Morton et al. 1956). Later on, the model was modified by including the thermal effects due to the temperature difference between the jet fluid and the density-stratified atmosphere.

The model is described here with reference to the formulation of Woods (1988). It includes the conservation equations of mass (Eq. 1), momentum (Eq. 2), and energy (Eq. 3), which are defined by means of the top-hat model. In the top-hat approximation, the fluid dynamic properties take one set of averaged values across the jet at any given height and another set of values for the ambient fluid; in this way, the flow parameters (velocity, density, radius, etc.) change only along the vertical direction z while remaining constant in the other directions. The conservation equations are as follows:

$$\frac{d\left(\rho_j U r^2\right)}{dz} = 2\rho_a r U_\varepsilon \tag{1}$$

$$\frac{d\left(\rho_j U^2 r^2\right)}{dz} = r^2 g\left(\rho_a - \rho_j\right) \tag{2}$$

$$\frac{d\left(\rho_j U r^2 \left(c_{p,j} T_j + \frac{U^2}{2} + gz\right)\right)}{dz} = 2U_\varepsilon r \rho_a\left(c_{P,a} T_a + gz\right) \tag{3}$$

where U is vertical jet velocity, r is column radius, ρ is bulk density, g is gravitational acceleration, c_P is the specific heat at constant pressure, T is temperature, z is the vertical coordinate, and the subscripts a and j refer to the surrounding atmosphere and jet, respectively. The quantity U_ε is the so-called entrainment velocity, which is defined as $U_\varepsilon = \varepsilon U$ (Morton et al. 1956), where ε is the entrainment coefficient.

The model was developed on the basis of the following assumptions: (1) the flow can be considered steady; (2) no pressure gradient exists between the jet fluid, which is assumed to behave as a perfect gas, and the surrounding atmosphere; (3) self-similarity of the field variables is respected, i.e., the profiles of mean vertical velocity and mean buoyancy force in the horizontal section of the flow have similar forms at any height (Morton et al. 1956); (4) particles can be considered as passive tracers and do not influence significantly fluid properties, e.g., density (Boussinesq approximation); (5) there is thermal and mechanical equilibrium between particles and jet fluid, which is a good approximation for fine particles with a large specific surface area and efficient heat exchange with the gas phase (Sparks et al. 1997); (6) all particles remain in the column, i.e., there is no particle segregation and deposition; (7) atmospheric effects, such as humidity (Woods 1993) and wind (Degruyter and Bonadonna 2013), are not accounted for.

Assumptions (4) and (5) lead to the definition of column characteristics and environment at any height by the "average" bulk macroscopic properties of velocity, density, and

temperature over the column cross-section (see Table 1 for the symbol list).

Table 1 Symbol notation

Symbol	Description	Units
A_{inflow}	Inflow surface area	m^2
C	Particle volumetric concentration	–
c_P	Specific heat at constant pressure	$J\ kg^{-1}\ K^{-1}$
D	Conduit diameter	m
d_{50}	Particle median grain size	mm
Fr_0'	Densimetric Froude number	–
g	Gravitational acceleration	$m\ s^{-2}$
g'	Reduced gravity	$m\ s^{-2}$
H	Height of the collapse of natural column	km
m	Mass of pyroclastic material	kg
MER	Mass eruption rate	$kg\ s^{-1}$
n	Gas mass fraction	–
P	Pressure	Pa
PMFR	Particle mass flow rate	$kg\ s^{-1}$
r	Jet radius	m
R	Specific gas constant	$J\ kg^{-1}\ K^{-1}$
Ri	Richardson number	–
SME	Specific mechanical energy	$J\ kg^{-1}$
T	Temperature	K
TMFR	Total mass flow rate	$kg\ s^{-1}$
U	Vertical velocity	$m\ s^{-1}$
U_ε	Entrainment velocity	$m\ s^{-1}$
V	Volume of gas	m^3
z	Vertical coordinate	m
z_{max}	Calculated maximum column height with the Bernoulli equation	m
$z_{max,an}$	Calculated maximum column height with the analytical solution	m
$z_{max,num}$	Calculated maximum column height with the numerical simulation	m
z_{obs}	Observed maximum column height	m
z_{ss}	Steady-state height	m
Γ_1	Regime parameter of Degruyter and Bonadonna (2013)	–
ΔP	Initial gas overpressure	Pa
ΔVFR	Increase of volume flow rate	$m^3\ s^{-1}$
ε	Entrainment coefficient	–
ρ	Density	$kg\ m^{-3}$
ϕ	Grain size	phi
Ω	Vorticity factor	s^{-1}
Subscripts		
0	Source conditions	
a	Surrounding atmosphere	
c	Centerline in a Gaussian profile velocity	
g	Gas	
j	Jet	
p	Solid particles	

Assumption (2) leads to the equation of state for the density of gas phase in the jet:

$$\rho_g = \frac{P}{RT} \qquad (4)$$

where P is fluid pressure, which is set equal to atmospheric value at any height by assumption (2), and R is the specific gas constant of gas phase in the eruptive flow, usually consisting of a multispecies gas mixture (e.g. CO_2, water vapor, etc.). Assumption (2) is not valid for eruptive jets issuing from the conduit with an overpressure with respect to the surrounding atmosphere (Ogden et al. 2008; Koyaguchi et al. 2010; Saffaraval et al. 2012). This can be the case for phreatomagmatic eruptions that generate eruptive clouds expanding radially above the vent and producing base surges (Koyaguchi and Woods 1996). This condition has been reproduced experimentally by the apparatus described in the following section (Dellino et al. 2010; Dioguardi et al. 2013), but the present paper deals only with pressure-balanced eruptive columns.

Assumption (5) leads to the constitutive equation of the gas-particle mixture density ρ_j:

$$\frac{1}{\rho_j} = \frac{1-n}{\rho_p} + \frac{n}{\rho_g} \qquad (5)$$

where ρ_p is the density of solid particles, and n is the gas mass fraction.

Finally, assumption (6) leads to the equation for the conservation of solid particle mass fraction $1-n$:

$$\rho_j U r^2 (1-n) = \rho_{j0} U_0 r_0^2 (1-n_0) \qquad (6)$$

where the subscript 0 refers to the vent exit conditions. It is assumed that there is no particle fallout from the column, although a formulation was developed to account for this process (Woods and Bursik 1991; Woods 2010).

From Eq. 6, it follows that the gas mass fraction n increases during column ascent, thus affecting the mixture specific heat at constant pressure c_{Pj}. A constitutive relationship linking the specific heat to the gas mass fraction is therefore required:

$$c_{P,j} = c_{P,a} + (c_{P,j0} - c_{P,a}) \frac{1-n}{1-n_0} \qquad (7)$$

where c_{Pa} is the specific heat at constant pressure of the atmosphere.

Finally, as the eruptive mixture entrains air from the surrounding atmosphere, the specific gas constant also varies as a function of the gas mass fraction:

$$R = R_a + (R_0 - R_a)\frac{1-n}{n}\frac{n_0}{1-n_0} \tag{8}$$

The entrainment velocity plays a major role in the evolution and spread of the flow during ascent. The concept of entrainment velocity stems from the original assumption of Morton et al. (1956), which has been successively verified experimentally, that the rate of lateral spread of the plume is proportional to the ascent velocity along plume axis; this assumption can be applied as long as the self-similarity condition is verified (assumption (3)). The top-hat approximation, from which the model discussed above derives, is a simplification of the Gaussian one, in which the radial profile of velocity is assumed to follow a Gaussian function, with U_c being the centerline velocity. This means that the centerline velocity U_c at any height is proportional to the entrainment velocity by the relation $U_\varepsilon = \varepsilon U_c$. The entrainment coefficient needs to be determined experimentally (e.g., Turner 1986) or theoretically (e.g., Carazzo et al. 2006, 2010). Here, we expand the concept of entrainment velocity and entrainment coefficient, as in the present paper they are calculated directly from experiments. A summary of the concepts and definitions of Turner (1986) is as follows: "The entrainment velocity is the rate, $U_\varepsilon = \varepsilon U_c$, at which external fluid flows into the turbulent flow across its boundary". As previously explained, in the top-hat model, the velocity and other physical quantities are assumed to be constant across the jet and zero outside (Morton et al. 1956), thus leading to $U_\varepsilon = \varepsilon U$. Morton et al. (1956) found a value of $\varepsilon = 0.132$ in the top-hat model, and $\varepsilon = 0.093$ for the Gaussian profile. See Turner (1986) for further details on the conversions between quantities of the top-hat model and those of the Gaussian model.

In the literature, the entrainment coefficient in the top-hat model is approximately equal to 0.06 for pure jets, whereas it is about 0.1 for pure plumes (Woods 1988, 2010; Bloomfield and Kerr 2000; Kaye and Hunt 2006; Carazzo et al. 2008, 2010; Papanicolaou et al. 2008). Given that the model of volcanic columns is used to follow the evolution in both the "gas-thrust" region, where buoyancy is negative, and in the much more extensive "convective buoyant" region, where buoyancy is positive, an average entrainment coefficient of 0.09 has been adopted in the literature (Woods 1988). More recently, variable entrainment coefficient laws have been introduced (Papanicolaou et al. 2008; Carazzo et al. 2008). These laws link the entrainment coefficient to the source densimetric Froude number Fr_0', a dimensionless fluid dynamic parameter that controls the regime of flows issuing from circular nozzles (Bloomfield and Kerr 2000; Kaye and Hunt 2006). Fr_0':

$$Fr_0' = \frac{U_0}{\sqrt{g_0' r_0}} = \frac{1}{\sqrt{Ri}} \tag{9}$$

where Ri is the local densimetric Richardson number (Carazzo et al. 2008; Suzuki and Koyaguchi 2012; Degruyter and Bonadonna 2013), and g_0' is the reduced gravity at the source, defined as follows:

$$g_0' = g\frac{\rho_{j0} - \rho_a}{\rho_a} \tag{10}$$

From 2D and 3D numerical simulations of eruption clouds, Suzuki et al. (2005) evaluated the entrainment rate of different eruptive scenarios (jets and collapsing clouds). Although they warn that the evaluation of the entrainment rate is significantly affected by the grid resolution, they found entrainment coefficients of 0.1 for buoyant columns and 0.07 (in the gas-thrust region) for negatively buoyant jets that evolve into collapsing columns. Here, we will show, by means of large-scale experiments and numerical simulations, that a collapsing column only forms when the entrainment rate ε is approximately equal to 0.

Morton-based models of the kind described above have been frequently applied to the eruption columns of past Plinian eruptions, but recent research in the fluid dynamics of negatively buoyant jets (Carazzo et al. 2006, 2008, 2010; Kaye and Hunt 2006; Papanicolaou et al. 2008; Suzuki and Koyaguchi 2012), corroborated by evidence from actual eruptions (Formenti et al. 2003; Carazzo et al. 2008), casts some doubts on their general validity, especially for the transitional conditions between Plinian plumes and collapsing columns. It seems that models based on Morton's theory work well for dilute plumes, where the seven assumptions described above seem more appropriate, but they do not work as well for dense collapsing columns forming pyroclastic density currents.

This issue could be attributed to the substantially lower entrainment coefficient that is needed for modeling dense negatively buoyant jets adequately, which is much less than those of both plumes (~0.1) and pure jets (~0.06). A reduction in the air entrainment leads to a less dilution of the column and, in turn, to greater heights reached due to the initial kinetic energy.

A precise definition of the entrainment coefficient is therefore of primary importance in the modeling of volcanic eruptive columns, as well as for hazard assessment purposes, as it influences the formation of fallout and pyroclastic density currents. Unfortunately, direct measurements of this quantity

are not practical for real eruptions. In order to cover this gap, we carried out large-scale experiments, specifically tailored for the volcanic case, with the aim of both comparing the characteristics of volcanic columns with those emerging from the recent fluid dynamics literature on jets and to directly measure the entrainment coefficient. By means of the experimental measurements, we compared the entrainment coefficients of dense jets generating collapsing columns with those of dilute gas-particle mixtures (both cold pure jets and hot plumes) generating pyroclastic fallout. Next, the experiments were simulated via a Fortran 90 numerical code of the model Eqs. 1–8, and numerical results were compared with experimental data. Finally, a threshold value of the initial densimetric Froude number leading to collapsing fountains vs. dilute plumes was obtained. This allows the construction of a diagram defining the stability fields of pyroclastic flow vs. fallout as a function of source conditions (exit velocity, conduit radius, and particle volumetric concentration).
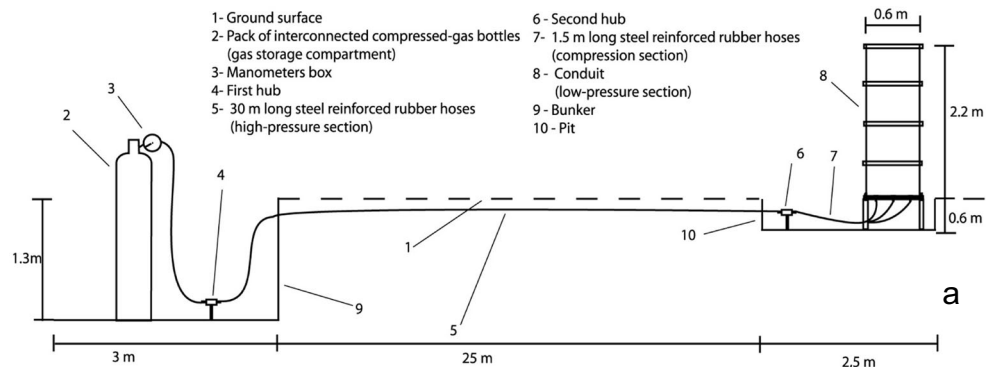
Large-scale experiments: setup and description

Large-scale experiments that generate eruptive columns producing plumes or collapsing fountains were carried out with the methods described by Dellino et al. (2007, 2010). Further

experimental runs have been carried out, and are included here, to increase the range of eruptive parameters already investigated in the previous papers.

The experiment design (Fig. 1) consists of a conduit that is loaded with up to 500 kg of samples of pyroclastic deposits from the Vesuvius, Etna, and Phlegrean Fields (southern Italy). The samples of Vesuvius come from pyroclastic flow deposits of the Pomici di Mercato eruption (8.9 ky BP, Mele et al. 2011). The median grain size is 0.65 ϕ (0.637 mm) with a sorting value of 2.5 ϕ. Particle densities, as obtained by picnometer measurements, range from 1,458 to 1,553 kg m^{-3}. The samples of Campi Flegrei come from pyroclastic flow deposits of the Astroni eruption (Unit 6, 4.1–3.8 ky BP, Isaia et al. 2004). The median grain size is 3.98 ϕ (0.063 mm) with a sorting value of 1.58 ϕ. Particle density is 2,408 kg m^{-3}, a value close to the dense rock equivalent as the particles are very fine, thus lacking in vesicles. The samples of Etna come from scoria deposits of the 2004–2005 eruption. The median grain size is −0.6 ϕ (1.48 mm) with a sorting value of about 1 ϕ; particle density is 1,045 kg m^{-3}. The experiment setup is modular and allows various parameters to be changed in order to replicate different eruptive regimes. The experimental apparatus, in its larger configuration, consists of up to two interconnected packs of 16 gas bottles (called the gas storage compartment, Fig. 1a); a

Fig. 1 Experiment design and main apparatus, after Dellino et al. (2007). **a** Experimental design; **b** general photograph of the pit where the second hub, solenoid valves, and the conduit are located. The base plate of the conduit is also shown. **c** General view of the conduit with the mounted pressure sensors and the additional 1-m long sector

1- Ground surface
2- Pack of interconnected compressed-gas bottles (gas storage compartment)
3- Manometers box
4- First hub
5- 30 m long steel reinforced rubber hoses (high-pressure section)
6 - Second hub
7- 1.5 m long steel reinforced rubber hoses (compression section)
8 - Conduit (low-pressure section)
9 - Bunker
10 - Pit

high-pressure section consisting of up to 18 steel-reinforced rubber hoses each 30 m long, with 8-mm internal diameter; a rapid-compression section consisting of up to 18 steel-reinforced rubber hoses each 1.5 m long, with 8-mm internal diameter; and a low-pressure section consisting of a steel conduit. Two conduits were used: a small one with a diameter of 0.3 m and a length of 1 m, which can be extended to 2 m by mounting an additional 1-m long section. A larger conduit consisted of a stack of sectors, each 0.55 m high with a diameter of 0.6 m, allowing the conduit length to range from 0.55 to 2.2 m and up to 3.2 m with the addition of another 1-m long section.

Experiments were performed both at ambient temperature and with the pyroclastic material heated up to 300 °C. For the gas phase, we used nitrogen in order to avoid the oxidation of the metallic parts of the setup (Dellino et al. 2007). The gas bottles were coupled to the high-pressure stage via two valves and a hub, in line with manometers that control the pressure in both the reservoir and the high-pressure section. High-speed solenoid valves connected the high-pressure section via a second hub to the rapid-compression section (Fig. 1b), where the driving pressure of the system is monitored by a transducer. The pressure transducer is mounted at the exit of the second hub after the solenoid valves. Finally, the short hoses are connected to 18 blow nozzles in the base plate of the low-pressure section (Fig. 1b). The nozzles cover up to 2 % of the total area of the base plate. The pyroclastic material was placed into the conduit (Fig. 1c) and rested directly on the base plate. The experiment was fully computerized: the opening of each solenoid, the trigger signal to the data acquisition systems, the start-up and shut down of high-speed cameras, and optical and acoustic warning signals were controlled with a reproducibility of 200 ms. A 24-channel data recording system was used at a resolution of 16 bit and at 10-kHz sampling rate, capturing the trigger signal from the control computer (giving the opening time of the solenoids), the driving pressure, and the signals from the sensor network recording flow parameters. The latter includes pressure sensors inside the conduit, pressure sensors for monitoring the passage of the pyroclastic flow, and electrostatic field sensors measuring the change in the electrostatic field around the conduit due to the fast acceleration/separation of pyroclastic particles inside the eruptive mixture. Four digital video cameras, positioned at different distances and viewing angles, were used to capture video sequences of the experiments. Thermal cameras were used to monitor the evolution of hot experiments.

The experiment starts by opening the valves that connect the gas storage compartment to the high-pressure section. By means of manometers, the pressure of the gas in the high-pressure section is controlled and regulated up to the desired operational value. When this value is reached, the valves are closed, and a charge of up to 28 L of compressed gas is loaded into the high-pressure section. After closure of the valves, the countdown routine of the control computer is started, the acquisition computers start recording signals from the sensors, and the cameras start recording the video footage. Upon firing of the trigger, the solenoid valves open, and a gas flow is established over 1 ms between the high-pressure section and the compression section, which results in the mechanical coupling of the pressurized gas to the pyroclastic material filling the conduit. The pressure quickly reaches a peak value in the compression section, and it remains quite constant for a brief period of time before a slow decompression phase is recorded (Dellino et al. 2010). In this phase, the pyroclastic material starts moving as a granular mass while it is accelerated inside the conduit, then it mixes with gas and overlying air, and eventually is expelled as a two-phase mixture out of the conduit. The driving pressure history, which is recorded by a transducer placed between the gas reservoir and the nozzles (Fig. 1b), was measured at a 10-kHz sampling rate by an absolute pressure sensor, which has a certified relative error of ±0.3 %. Transducers placed within the conduit perpendicular to flow direction allowed measurement of gas pressure during the passage of the gas-particle mixture along the conduit (see Dellino et al. 2010). Gas pressure was recorded at a 1-kHz sampling rate by relative pressure sensors, which have a certified relative error of ±0.25 %. Depending on the balance between the operational pressure of the compressed gas volume in the high-pressure section and the mass of pyroclastic material, different eruptive processes were replicated.

The ratio $\Delta PV/m$, where ΔP is the initial gas overpressure (i.e., pressure>atmospheric) in the high-pressure section, V is the volume of the gas charge in the high-pressure section, and m is the mass of pyroclastic material, accounts for the specific mechanical energy (SME) of the system (Dellino et al. 2007). It represents the gas potential to move the mass of pyroclastic material. When SME is lower than 1.5 kJ kg^{-1}, the "eruptive" flow evolves as a dense (high particle concentration) column. In this case, a massive collapse of a substantial part of the gas-particle column occurs (Fig. 3), and on impact with the ground, the collapsing material produces a shear flow, similar to a pyroclastic flow. When the SME is higher than about 2.6 kJ kg^{-1}, the eruptive flow evolves as a low-density (low particle concentration) vertical column (Figs. 4, 5), no massive collapse occurs, and the pyroclastic particles settle individually from the column margin, similar to fallout from a volcanic plume.

For the present paper, detailed measurements of velocity and geometric characteristics of the eruptive columns were obtained from the analysis and post-processing of digital videos from the cameras that recorded flow evolution from different distances and viewing angles.

The high-definition video format (720×1,280 pixels) allowed discretization of the scene at the conduit exit at a scale less than 0.01 m pixel^{-1}, so the precision of spatial

measurements was about ±0.005 m. The recording rate of 50 frames s^{-1} resulted in a typical translation distance of the gas-particle mixture at a conduit exit of about 0.5 m between two successive frames (depending on exit velocity). The relative error on distance measurements between two successive frames is therefore about ±1 %. The error on the time interval between two successive frames is linked to the precision of the internal digital clock of video cameras and is insignificant compared to distance error. Overall, the relative error of velocity measurements is about ±1 %.

Thermal cameras were used to monitor the formation of buoyant columns (plumes) that occurred for the low particle concentration, high temperature runs (Fig. 2). By means of this setup, the maximum height of the column for collapsing fountains, and the maximum height where initial momentum (kinetic energy) was consumed (height of transition between initial momentum driven flow and thermally buoyant flow), were measured.
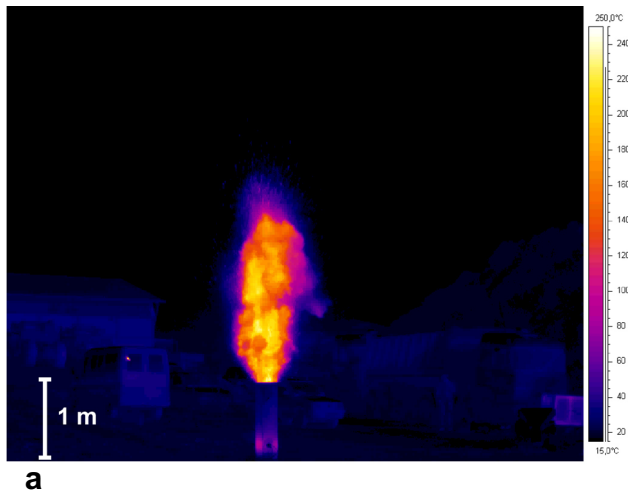
Fig. 2 Thermal images of a high temperature run forming a buoyant plume. Temperatures are in °C. **a** Formation of the eruptive column at conduit exit. **b** Spread of the column and thermal convection

The flow evolution inside the conduit, and up to conduit exit, was monitored by a sensor network (for the complete dataset see Dellino et al. 2010; Dioguardi et al. 2013), which allowed selection of runs for which the gas-particle mixture issued from the conduit at a pressure equal to that of the surrounding atmosphere (to satisfy assumption (2) of the "Introduction" section). The particle mass flow rate $PMFR_0$ at the conduit exit was calculated by knowing the total mass of particles and the duration of gas-particle flow exiting the conduit. The particle mass flow rate was assumed to be steady during the experiment, since the gas flow rate entering the conduit, as recorded by a high precision high frequency pressure transducer, was found to be constant.

By knowing the particle mass flow rate, exit velocity, and conduit diameter and assuming that gas and particle velocities were in equilibrium (reasonable for fine particles, assumption (5) of the "Introduction" section), the source particle volumetric concentration can be calculated from

$$C_0 = \frac{PMFR_0}{\pi r_0^2 U_0 \rho_p} \tag{11}$$

where r_0 is the conduit radius, and U_0 is the gas-particle mixture exit velocity. From the conservation of volume, the gas concentration is $1\text{-}C_0$, the gas-particle mixture density at conduit exit ρ_{j0} is given by

$$\rho_{j0} = \rho_p C_0 + \rho_g (1\text{-}C_0) \tag{12}$$

and the total mass flow rate $TMFR_0$ is given by

$$TMFR_0 = U_0 \rho_{j0} \pi r_0^2 \tag{13}$$

In the experiments, samples from pyroclastic deposits of the Mercato eruptions at Vesuvius (Dellino et al. 2007, 2010) were mostly used. The grain size distribution is broad with a median size d_{50} of about 1 mm. For assessing the influence of grain size, also some samples from the Etna scoria (d_{50}= 1.48 mm) and Phlegrean Fields' fine ash (d_{50}=0.063 mm) were used (Table 2).

The particle loads of experimental runs ranged between 10 to 500 kg, resulting in particle volumetric concentrations, C_0, at conduit exit ranging from 0.002 to 0.16 and exit velocities, U_0, in the range 5 to 35 m s^{-1} and total mass flow rates, $TMFR_0$, in the range 5 to 338 kg s^{-1}. The Reynolds number was in the order of 10^6, meaning that fully turbulent flows were produced at the conduit exit. These conditions ensure that the experiments are dynamically similar to real eruption columns (Dellino et al. 2010). A total of 26 experimental runs form the dataset used in this paper, which is shown in Table 2.

Table 2 Experimental data and results

Experiment	Material	d_{50} (mm)	ρ_P (kg m^{-3})	U_0 (m/s)	$TMFR_0$ (kg s^{-1})	C_0	$\rho_{f,0}$ (kg m^{-3})	Fr_0'	r_0 (m)	z_{ss} (m)	z_{ss}/r_0	z_{obs} (m)	z_{max} (m)	$z_{max,an}$ (m)	ε	$z_{max,num}$ (m)
1	Mercato	0.637	1552.88	12.10	337.51	0.0628	98.62	0.79	0.30	4.28	14.27	6.12	7.46	7.55	n.s.	7.55
2	Mercato	0.637	1552.88	10.95	289.49	0.0595	93.47	0.73	0.30	3.46	11.54	4.95	6.11	6.19	n.s.	6.19
3	Mercato	0.637	1552.88	11.12	337.17	0.0683	107.20	0.70	0.30	4.22	14.08	6.04	6.30	6.37	n.s.	6.37
4	Mercato	0.637	1552.88	10.33	281.34	0.0613	96.29	0.68	0.30	3.97	13.22	5.67	5.44	5.51	n.s.	5.51
5	Mercato	0.637	1552.88	8.78	73.44	0.0757	118.67	0.74	0.15	1.44	9.63	4.13	3.93	3.97	n.s.	3.97
6	Mercato	0.637	1552.88	6.32	90.27	0.1295	202.11	0.41	0.15	0.73	4.87	2.09	2.03	2.05	n.s.	2.05
7	Mercato	0.637	1552.88	8.67	72.98	0.0762	119.43	0.73	0.15	1.50	10.02	4.13	3.83	3.87	n.s.	3.87
8	Mercato	0.637	1552.88	6.95	87.23	0.1139	177.93	0.48	0.15	1.03	6.88	2.95	2.46	2.48	n.s.	2.48
9	Mercato	0.637	1552.88	5.10	87.28	0.1553	242.21	0.30	0.15	0.47	3.10	1.33	1.32	1.33	n.s.	1.33
10	Mercato	0.637	1458.85	7.48	87.49	0.1126	165.40	0.38	0.30	2.10	6.99	3.00	2.85	2.87	n.s.	2.87
11	Mercato	0.812	1458.85	14.42	194.45	0.0319	47.67	1.36	0.30	7.63	25.43	10.91	10.60	10.87	n.s.	10.87
12	Mercato	0.812	1458.85	12.77	196.90	0.0366	54.51	1.13	0.30	6.70	22.34	9.59	8.31	8.50	n.s.	8.50
13	Mercato	0.812	1458.85	13.33	215.31	0.0383	57.10	1.15	0.30	6.32	21.06	9.04	9.06	9.25	n.s.	9.25
14	Phlegrean Fields	0.063	2408.00	11.36	195.95	0.0248	61.01	0.95	0.30	5.13	17.09	7.33	6.58	6.71	n.s.	6.71
15	Phlegrean Fields	0.063	2408.00	17.50	231.04	0.0189	46.69	1.67	0.30	10.19	33.96	14.57	15.61	16.02	n.s.	16.01
16	Mercato	0.812	1458.85	16.30	230.62	0.0335	50.02	1.50	0.30	8.81	29.37	12.60	13.54	13.87	n.s.	13.86
17	Mercato	0.637	1552.88	13.23	5.23	0.0031	5.59	5.76	0.15	3.06	20.42	4.38	8.92	11.36	0.12	3.99
18	Mercato	0.637	1552.88	11.67	4.58	0.0031	5.56	5.10	0.15	3.29	21.96	4.71	6.94	8.85	0.12	4.08
19	Etna	1.480	1045.00	8.72	5.30	0.0075	8.59	2.92	0.15	1.89	12.59	2.70	3.88	4.50	0.10	4.88
20	Mercato	0.637	1552.88	12.54	4.61	0.0026	5.20	5.72	0.15	3.15	20.98	4.50	8.01	10.42	0.06	6.12
21	Mercato	0.637	1552.88	10.56	4.83	0.0034	6.47	4.20	0.15	2.45	16.36	3.51	5.68	6.98	0.06	4.85
22	Mercato	0.637	1552.88	14.46	33.40	0.0045	7.73	3.65	0.3	4.68	15.59	6.69	10.66	12.61	0.06	9.34
23	Mercato	0.812	1458.85	26.40	73.50	0.0047	7.63	6.71	0.3	6.69	22.28	9.56	35.52	42.15	0.11	10.15
24	Mercato	0.812	1458.85	28.57	60.64	0.0043	7.07	7.61	0.3	8.23	27.44	11.77	41.60	50.11	0.12	12.14
25	Mercato	0.812	1458.85	35.11	63.04	0.0035	5.91	10.44	0.3	10.41	34.71	14.89	62.83	78.83	0.10	12.15
26	Phlegrean Fields	0.063	2408.00	25.40	39.98	0.0020	5.57	7.84	0.3	8.01	26.69	11.45	32.88	41.92	0.11	10.65

n.s. not significant, *i.e.* not significantly different from 0

The different eruption regimes produced in the experiments can be grouped into two main categories: (1) experiments with higher initial particle volumetric concentrations (and higher mass flow rates), which produced dense columns (Fig. 3a) that collapsed to the ground and generated intense shear currents (Fig. 3b), similar to volcanic pyroclastic density currents; (2) experiments with lower particle volumetric concentrations that generated expanded columns (both hot, Fig. 4a, b and cold, Fig. 5a, b), with particles settling individually from their margins, similarly to volcanic pyroclastic fallout.

The experiments lasted for few seconds, and the gas-particle flow at the conduit exit lasted longer than the time needed for the column to reach its maximum height due to the initial kinetic energy. Therefore, the flow can be considered steady (assumption (1) of the "Introduction" section), as stated in Dioguardi et al. (2013). Some variation of particle flow rate at the conduit exit probably occurred during the final stage of flow, but this "perturbation" at the source did not influence the dynamics higher up in the column (at a distance greater than 10D, where D is the conduit diameter; Fischer et al. 1979; Turner 1986).

Experiment results and analysis

The two groups of experiments described in the previous section (generating dense and expanded columns) are visually very different, and the difference can be evaluated quantitatively by assessing the conservation of mechanical energy from conduit exit to maximum height. Since pressure is equivalent to energy per unit volume, this can be done by verifying the conservation of total pressure at any height, as prescribed by Bernoulli's equation:

$$\frac{1}{2}\rho_{j0}U_0^2 + \rho_{j0}gz = \text{const} \tag{14}$$

Assuming constant density, Eq. 15 leads to

$$z_{\max} = \frac{U_0^2}{2g} \tag{15}$$

The relationship between the observed height z_{obs} and that calculated by assuming energy conservation $z_{\max}$ (Eq. 15) shows the different behaviors between the two groups of experiments (Fig. 6). For group 1, (diamonds in Fig. 6) there is a good agreement between the calculated and observed heights, with the data points lying on the equality line (solid line), which means that the total pressure conservation prescribed by Bernoulli's equation is satisfied. This also means that in the experiments producing collapsing columns and pyroclastic density currents, mixture density is conserved throughout the flow, and that the initial kinetic energy is completely converted into potential energy. Therefore, for the dense columns, there is no apparent energy loss by friction with the surrounding fluid and by air entrainment. This is confirmed by solving Eqs. 1 to 6 in the case of no entrainment, i.e., $U_\varepsilon = \varepsilon U = 0$: the system of equations simplifies and, upon assuming a constant atmospheric pressure in the vertical direction (which is a good approximation for our experiments)

Fig. 3 Images of an experimental dense column. **a** Formation of the dense column at conduit exit. **b** Collapse of the dense column with the formation of a density current
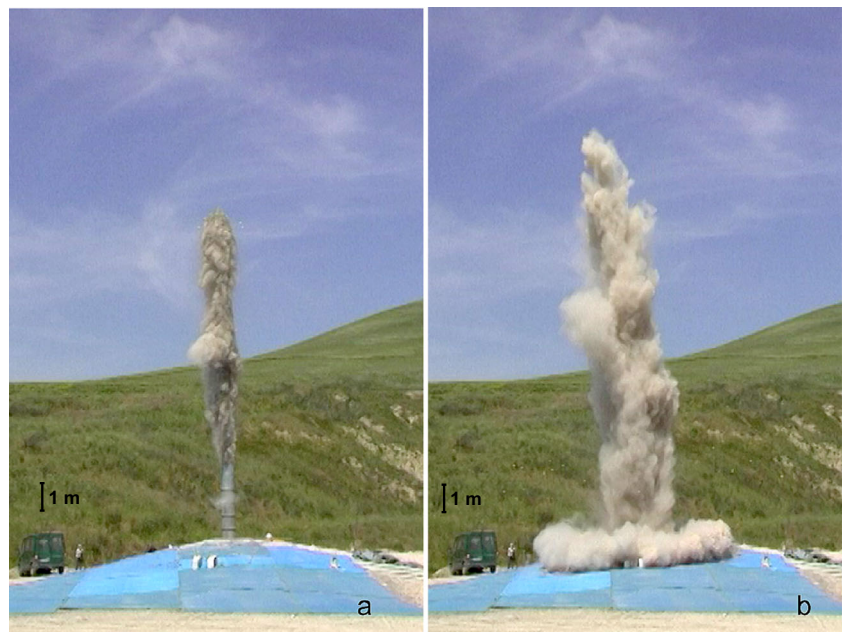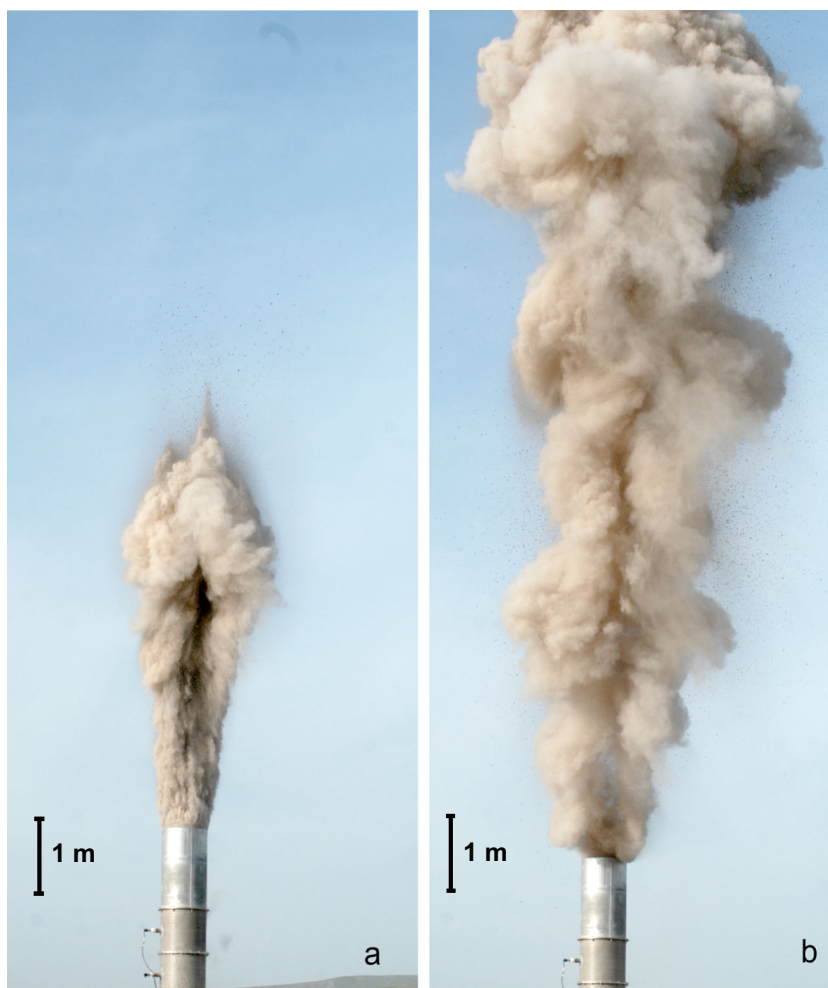
Fig. 4 Images of an experimental dilute hot column. **a** Formation of the dilute hot column at conduit exit. **b** Spread of the dilute hot column and formation of the plume

and again a constant density, the equations can be solved analytically. The analytical solution for the mixture velocity is

$$U = \pm\sqrt{2}\sqrt{\frac{g\left(\rho_g - \rho_j\right)}{\rho_j}z + \frac{U_0^2}{2}} \qquad (16)$$

With the boundary condition $U=0$ at $z=z_{\mathrm{max,an}}$, the maximum height in the case of zero entrainment is

$$z_{\mathrm{max,an}} = \frac{U_0^2}{2g\dfrac{\rho_j - \rho_g}{\rho_j}} \qquad (17)$$

The results of the analytical solution are nearly identical to those obtained with Bernoulli's approximation for the dense experiments generating collapse (the average difference is about 2 %, see Table 2). The small difference is due to the ratio $(\rho_j - \rho_g)/\rho_j$, which in Bernoulli's solution (15) is not taken

into account. For the dense column experiments, this ratio is always slightly larger than 1, as the mixture density ρ_j is 2–3 orders of magnitude larger than the gas density ρ_g.

The behavior of group 2 experiments (square symbols in Fig. 6) is much different. The observed height reached before the onset of buoyancy is much smaller than that prescribed by Bernoulli's equation, and the data points are far from the equality line, especially for the higher velocities. This implies that there is a significant energy loss by friction and air entrainment, which is also apparent by the much more expanded form of the column as compared to group 1 experiments (see Figs. 4 and 5). We note that both hot dilute columns (Fig. 4) and cold dilute columns (Fig. 5) spread significantly during ascent compared to dense columns. For the cold dilute columns, there is no collapse but simply fallout from column margin, which means that even when thermal buoyancy is not active, the dilution effect of the spreading column precludes the formation of a dense collapsing fountain.

The densimetric Froude numbers (Eq. 9) calculated for group 1 and group 2 experiments are quite different (Table 2), which allows dense columns generating pyroclastic
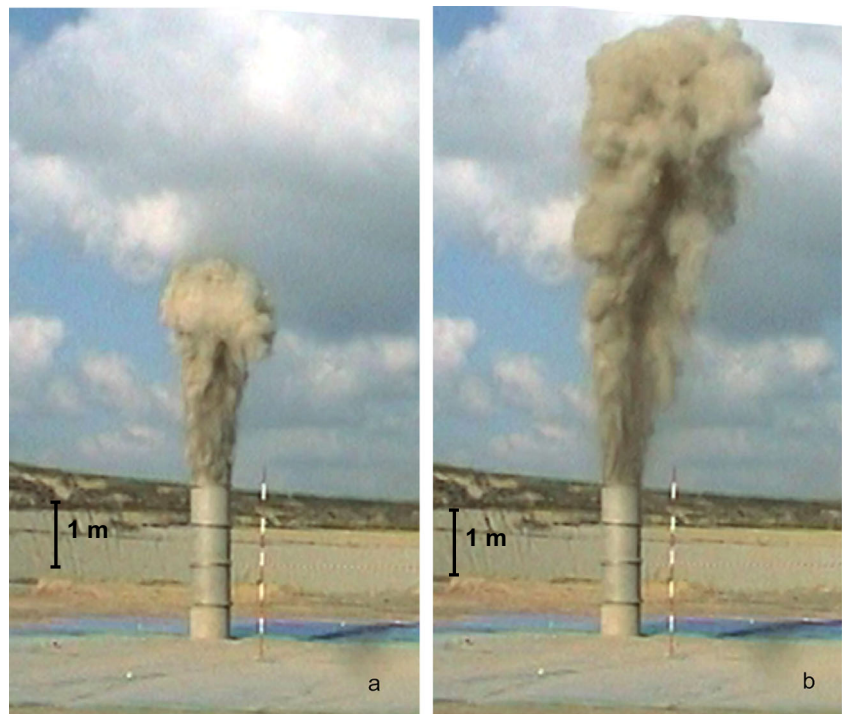
density currents to be discriminated from dilute columns
generating fallout. By analogy with the recent literature on
negatively buoyant jets (e.g., Kaye and Hunt 2006), the data
from our experiments are plotted on a diagram of normalized
height (ratio between the final steady-state height z_{ss} and
conduit radius) vs. the initial densimetric Froude number
(Fig. 7). The value of z_{ss} is calculated as the ratio of the
observed maximum height z_{obs} and 1.43, according to the
literature on negatively buoyant jets (Turner 1966; Kaye and
Hunt 2006). For collapsing columns (both hot and cold), the
relationship between the Froude number (which is always less
than 3) and the normalized height is linear, with a very good
correlation ($r=0.99$). Dilute columns (both hot and cold)
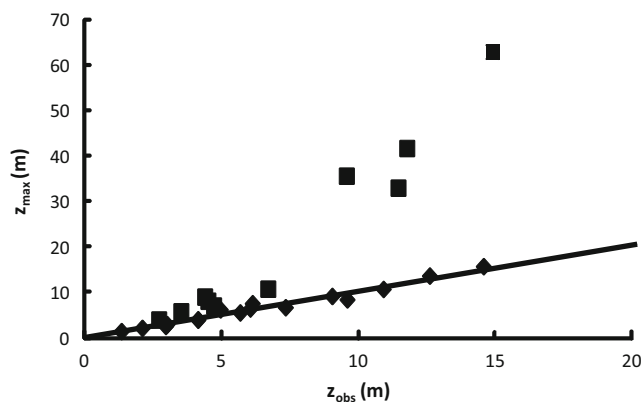
Fig. 6 Diagram of the maximum height calculated with Bernoulli's
equation (z_{max}) vs. the observed maximum column height resulting from
the initial kinetic energy (z_{obs}). *Squares* represent dilute columns,
diamonds represent dense columns. The 1:1 equality line is shown

leading to pyroclastic fallout (group 2 experiments) have
Froude numbers greater than about 3, and data show a linear
relationship with a very good correlation ($r=0.99$) and a much
lower slope (2.9) than that of group 1 (22.4). Figure 7 shows
the clear separation between the two groups of experiments. It
is worth noting that Kaye and Hunt (2006) discriminate weak
fountains from forced jets based exactly on the same threshold
value Fr_0'; and for weak fountains, they found that the en-
trainment rates are much less than those of pure jets and
plumes. The slope (2.9) of the linear relationship found for
our "dilute" experiments (group 2) is similar to that (2.46)
found for forced jets by Kaye and Hunt (2006). The value of
the intercept in our case (about 5) is larger than that reported in
Kaye and Hunt (2006) (about 0.4). This difference is likely to
be attributed to the different ranges of Fr_0' investigated: for
our group 2 experiments, Fr_0' ranges between 3 and 11, while
in Kaye and Hunt (2006), the maximum Froude number was
about 200. The relationship between the initial densimetric
Froude number and the normalized height for the "dense"
experiments (group 1, Fr_0'<3) is linear in our case. This is
different from the data reported by Kaye and Hunt (2006),
which suggest a quadratic relationship. However, other au-
thors (Lin and Armfield 2000) maintain a linear relationship.
We note that our experiments at low initial densimetric Froude
number (collapsing columns) have a reduced gravity that is
significantly greater than that used in engineering experiments
(e.g., Carazzo et al. 2006, 2010; Papanicolaou et al. 2008) and
simulations (e.g. Lin and Armfield 2000). It is likely that this
can cause the difference in the coefficients of the relationship
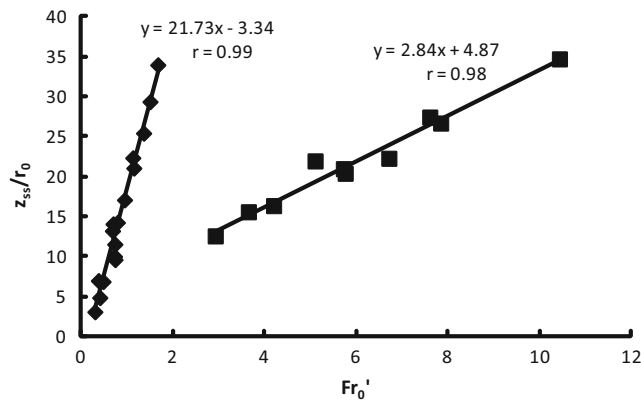with the normalized height.

Fig. 7 Diagram of the normalized height (z_{ss}/r_0) vs. the initial densimetric Froude number (Fr_0'). *Squares* represent dilute columns, *diamonds* represent dense columns. The least square lines of both dilute and dense columns are shown, together with the correlation coefficients, r, and the equation of the regression lines

To summarize, our experiments suggest that the entrainment of external air seems to be insignificant in the case of collapsing columns forming pyroclastic density currents, whereas it is important for dilute expanded columns (both cold and hot) producing pyroclastic fallout.

To further corroborate this result, we measured the entrainment coefficient by means of a quantitative analysis of experiment video recordings.

As already stated in the "Introduction" section, the entrainment coefficient is defined as the ratio between the entrainment velocity U_ε and the ascent velocity U, which in the top-hat approximation coincides with the centerline velocity U_c. The entrainment velocity was calculated by dividing the increase of volume flow rate, ΔVFR, by the surface area of the boundary of air inflow A_{inflow}:

$$U_\varepsilon = \frac{\Delta VFR}{A_{\inf\ low}} = \frac{(U\pi r^2)z_1}{2\pi r_{z_2}(z_2-z_1)} \qquad (18)$$

where z_1 and z_2 are two successive heights. The entrainment coefficient was calculated as the ratio of entrainment velocity and vertical velocity at z_2.

The measurements were made by analyzing video of the experiments, after the column had reached a height of about $10D$. Velocity was calculated as the average of five successive frames, and the two successive heights were taken at a distance of at least 0.5 m, to minimize sampling error. Results are reported in Table 2.

In Fig. 8, two examples of entrainment velocity measurements are displayed, one for dense fountains (Fig. 8a) and one for hot dilute plumes (Fig. 8b); the difference between the two cases is quite marked, as the spreading rate of the dilute column is much greater than that of the dense column.
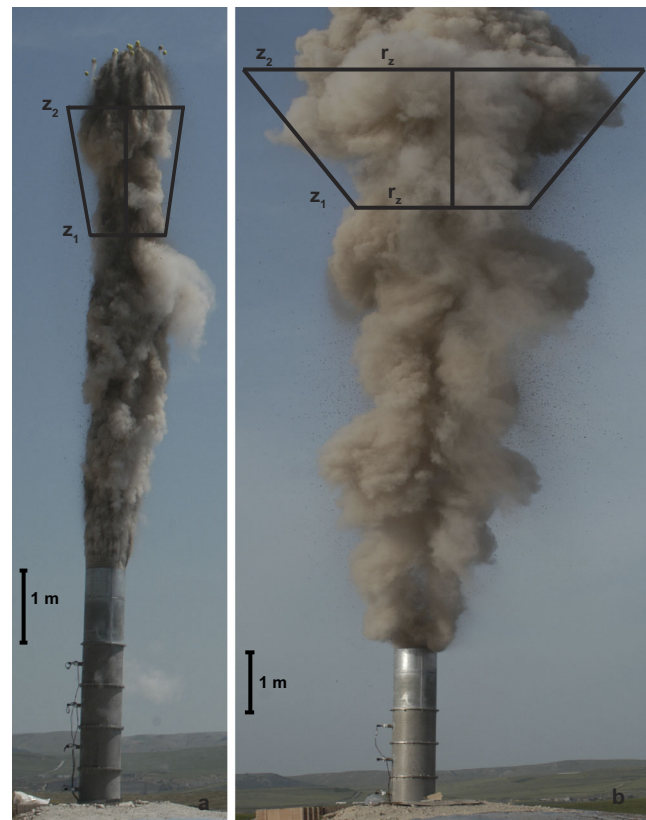

Fig. 8 Measurement of the parameters needed for the calculation of the entrainment velocity U_ε. **a** Dense fountain. **b** Hot dilute column. The two heights z_1 and z_2 and the jet radius as a function of the height r_z are displayed

The entrainment coefficient of collapsing columns (group 1) is not significant, as expected. In fact, it ranges between 0.0007 and −0.0007 (Fig. 8a), the deviation from zero being within the experimental error of measurements (in the range of 1 %, see Dellino et al. 2007). For cold dilute columns (cold runs of group 2), which can be considered similar to pure jets, the average entrainment coefficient was about 0.06, which is quite consistent with data from fluid dynamic engineering (Bloomfield and Kerr 2000; Kaye and Hunt 2006; Carazzo et al. 2008, 2010; Papanicolaou et al. 2008). The entrainment coefficient of hot dilute columns (hot runs of group 2) generating buoyant columns is on average about 0.11 (Fig. 8b), which is consistent with data from plumes reported in the fluid dynamics and volcanological literature (Woods 1988; Kaye and Hunt 2006; Carazzo et al. 2008, 2010).

Numerical simulation of experiments

In order to verify the compatibility of our experimental measurements of the entrainment coefficient with the top-hat model illustrated in the "Introduction" section, the system of Eqs. 1–8 was solved with a numerical code written in Fortran 90. The code uses the 4th order Runge-Kutta method of

integration of ordinary differential equations with a constant step-size (Press et al. 1996). The boundary conditions needed for the simulation of each experiment are the initial column radius r_0, fluid velocity U_0, fluid temperature T_0, and particle volumetric concentration C_0 at the conduit exit (see Table 2). The thermodynamic quantities needed for the solution of Eqs. 3, 4, 7, and 8, are listed in Table 3. Atmospheric temperature, T_a, is kept constant at 25 °C (298 K), the specific gas constant R_a is 287.05 J kg^{-1} K^{-1}, and the specific heat at constant pressure $c_{P,a}$ is 1,005 J kg^{-1} K^{-1}. For the gas (nitrogen), the temperature is by default equal to the source fluid temperature T_0, the specific gas constant R_0 is equal to 271.75 J kg^{-1} K^{-1}, and the specific heat at constant pressure $c_{P,g}$ is equal to 1,042 J kg^{-1} K^{-1}. In order to calculate the source specific heat at a constant pressure of the jet bulk mixture $c_{P,j0}$, the specific heat of the solid particles $c_{P,s}$ is necessary. We chose a value of $c_{P,s}=1{,}617$ J kg^{-1} K^{-1} for consistency with other authors (Woods 1988; Formenti et al. 2003; Suzuki and Koyaguchi 2009).

The source specific heat at constant pressure of the jet bulk mixture $c_{P,j0}$ is obtained as a weighted average between the gas and the solid phases:

$$c_{P,j0} = \frac{(1-C_0)\rho_{g0}c_{P,g0} + C_0\rho_p c_{P,s}}{(1-C_0)\rho_{g0} + C_0\rho_p} \qquad (19)$$

As output, the code provides the vertical profiles of column velocity, radius, bulk density, and temperature, together with atmospheric temperature, density, and particle volumetric concentration.

For the entrainment coefficient, ε, which is crucial for the evolution of the eruption column, we used the values measured by experiments (Table 2) as model inputs to check whether the numerical simulations produced results, i.e., velocity and maximum height, consistent with experimental data. To demonstrate that the numerical simulations replicate the experimental flow evolution, Fig. 9a shows model vertical profiles of column radius (solid line) and velocity (dashed line) obtained using input data from experiment 3 (Table 2)

Table 3 Physical constants used in the numerical simulations

Symbol	Description	Value
T_a	Temperature of the atmosphere	298 K
R_a	Specific gas constant of the atmosphere	287.05 J kg^{-1} K^{-1}
$c_{P,a}$	Specific heat at constant pressure of the atmosphere	1,005 J kg^{-1} K^{-1}
R_0	Specific gas constant of nitrogen	271.75 J kg^{-1} K^{-1}
$c_{P,g}$	Specific heat at constant pressure of nitrogen	1,042 J kg^{-1} K^{-1}
$c_{P,s}$	Specific heat at constant pressure of solid particles	1,617 J kg^{-1} K^{-1}

as an example of a collapsing column. As the vertical velocity decreases with increasing height (due to the strong negative buoyancy), the column radius increases due to the conservation of volume. At the height $z_{max,num}$, the velocity goes to 0: this is the height at which kinetic energy is consumed and the column stops ascending. The $z_{max,num}$ value is similar to the experimental value z_{obs} (Table 2), which implies that simulations with no entrainment replicate well the behavior of the collapsing experimental columns. We note that after the column stops ascending, collapse occurs during the experiments, whereas the numerical simulation calculates an infinite radius at the maximum height, in order to satisfy the conservation of mass flow when the velocity drops to zero (Eq. 1). This is a well-known limitation of column models based on the Morton et al. (1956) theory, but it does not influence the calculation until the column reaches its maximum height.

In Fig. 9b, the numerical simulation of the dilute column of experiment 24 (Table 2) illustrates the differences from the collapsing column of Fig. 9a. In particular, the rate of increase of column radius with increasing height is much larger for the dilute column than for the dense fountain, as there is the additional contribution of air entrainment, which in this case results from an entrainment coefficient of 0.12. This is in agreement with the experimental measurements and observations (Fig. 8). The velocity of this plume never falls to 0, as at the height $z_{max,num}$, the jet reaches the condition of buoyancy, i.e., the column bulk density becomes less than that of the atmosphere (Fig. 9c). In contrast, the buoyancy condition was never reached in the case of collapsing fountains, due to the much higher source density and to the lack of turbulent mixing with atmosphere. The height at which the model plume density equals that of the atmosphere is in good agreement with that measured in the experiment (Table 2). This means that, by using the experimentally measured entrainment coefficients in the model, the numerical simulation satisfactorily replicates the experimental plume evolution with height.

In the dilute experiments carried out at ambient temperature (runs 20, 21, and 22 of Table 2), which never achieved buoyant conditions, the measured entrainment coefficient is about 0.06 and the particle volumetric concentration is quite low ($C_0<0.01$). In these cases, $z_{max,num}$ is taken as the height at which $U=0$, as in the case of collapsing fountains. The model correctly replicates the cold dilute runs if the experimentally measured entrainment coefficient of 0.06 is used.

The case of dilute cold experiments deserves some additional comment that can provide insights into the interpretation of volcanic jets. The entrainment coefficient of 0.06 for cold dilute experiments is lower than that of thermally buoyant plumes, but is consistent to those reported for pure jets in the fluid dynamics literature (Turner 1986; Kaye and Hunt 2006; Carazzo et al. 2008).

This means that in our dilute hot experiments, as with real volcanic plumes, the thermal effect is of fundamental

Fig. 9 Typical vertical profiles of vertical velocity of the bulk mixture (*U*, *dashed lines*) and column radius (*r_j*, *solid lines*) as calculated by the numerical model for a dense collapsing column (**a** experiment 3 of Table 2) and for a dilute hot column (**b** experiment 24 of Table 2). **c** Vertical profiles of bulk column density (*solid line*) and atmospheric density (*dashed line*) in the case of a dilute hot column (experiment 24)
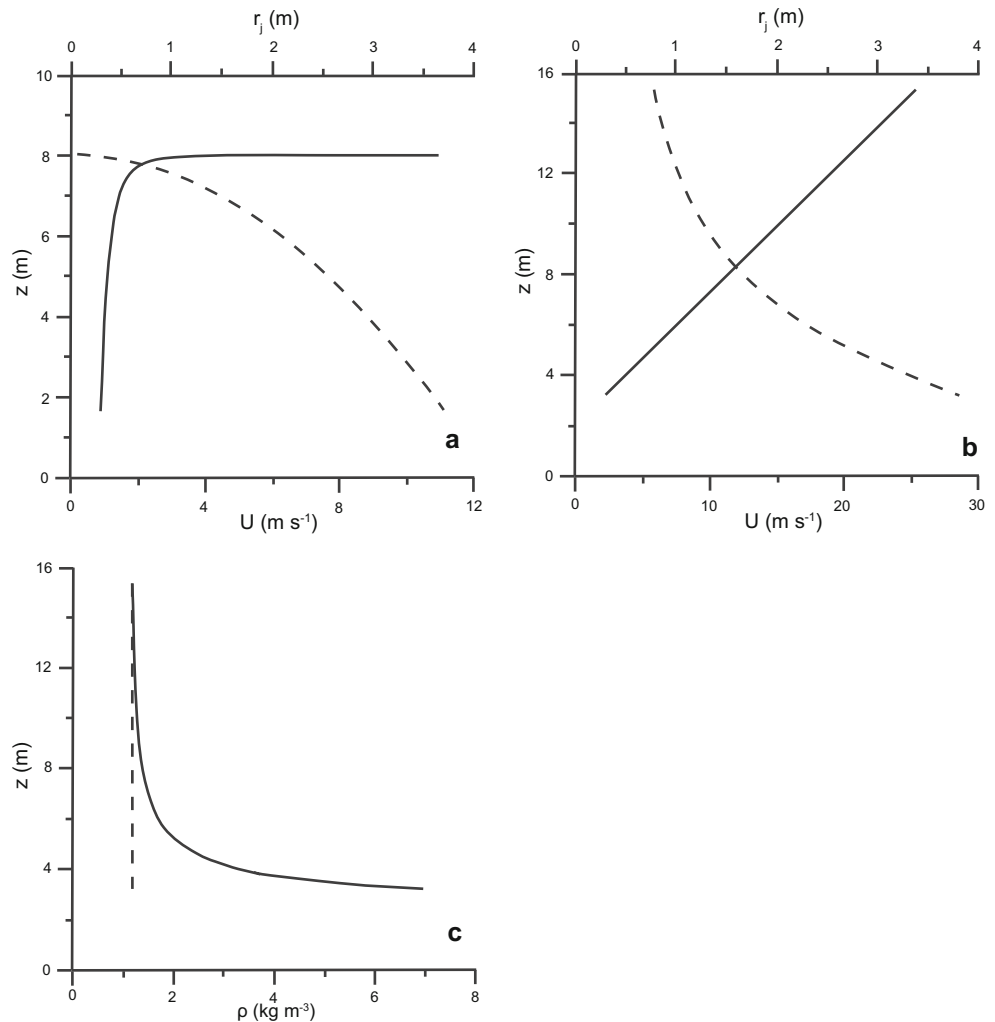
importance for producing the higher entrainment coefficient (about 0.11) of true buoyant plumes. However, air entrainment also affects the cold dilute experimental jets, even though they are in thermal equilibrium with the surroundings. Thus, entrainment occurs also in the case of pure forced convection, if particle concentration is low. The cold jets do not reach buoyancy, but neither do the they evolve into collapsing fountains. Although the entrainment rate is lower than that of the hot jets (evolving into buoyant plumes), dilution is sufficient in expanding the gas-particle mixture so that a "massive" collapse does not occur. In this case, particles fall down from the column margins. Therefore, it can be concluded that collapsing fountains forming pyroclastic flows result only from dense eruptive columns that lack significant air entrainment. This is in agreement with the condition for column collapse presented by Degruyter and Bonadonna (2013): if *ε* is equal to 0, the parameter

$$\Gamma_1 = \frac{-Ri}{\varepsilon} \quad (20)$$

tends to infinity, forcing any eruptive scenario to fall into the collapsing column stability field (see Fig. 2 of Degruyter and Bonadonna (2013)).

In order to assess the general agreement between experiments and numerical simulations, Fig. 10 shows the maximum height due to initial momentum ($z_{max,num}$) calculated by the model, plotted against the maximum height due to initial kinetic energy (z_{obs}) measured by experiments. Data for all the runs of Table 2 are shown. The maximum observed height of the experiments is predicted well by the numerical model ($r=0.95$, Fig. 10). Thus, the model reproduces correctly the experimental column evolution if the actual entrainment coefficient, as measured experimentally, is used. Furthermore, in the case of no entrainment (collapsing fountains), the numerical model reproduces almost exactly the analytical solution proposed in the "Experiment results and analysis" section (see Table 2). Therefore, for dense collapses, the numerical solution and that obtained from Bernoulli's equation give similar results.
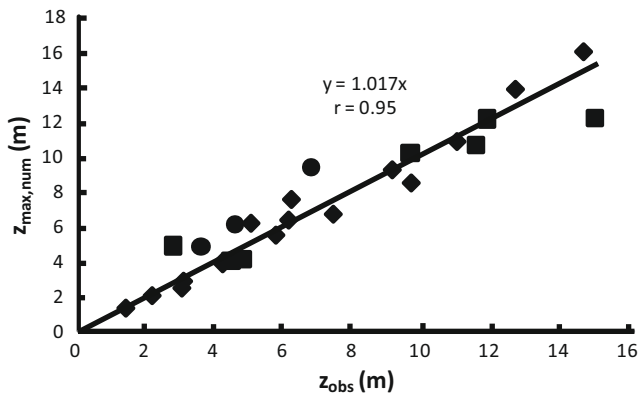
Fig. 10 Comparison between the maximum height reached by initial momentum calculated by the numerical model $z_{max,num}$ and the maximum observed height resulting from the initial kinetic energy in the experiments z_{obs}. *Diamonds* represent dense collapsing fountains with no entrainment; *circles* represent cold dilute columns (for the entrainment coefficient, see Table 2); *squares* represent hot dilute columns (for the entrainment coefficient, see Table 2)

Relevance of experimental and numerical results to natural volcanic columns and conclusive remarks

Due to the technological limitations in inspecting the internal structure of opaque multiphase gas-particle flows, the experimental measurements presented in this paper lack the details of the internal gradients of velocity and particle volumetric concentration in the eruptive column. However, the facility we used allowed acquisition of results that shed new light on the eruptive regime of buoyant volcanic plumes and collapsing fountains. Our experiments produced fully turbulent flows, for which conduit exit velocity, particle volumetric concentration, and column height were measured. The new data allowed the application of fluid dynamic scaling laws that helped to constrain the eruptive conditions leading to pyroclastic flows vs. fallout.

To our knowledge, there are no other large-scale experiments specifically tailored for the case of gas-pyroclast mixtures with which to compare our data. It was therefore hard to find a way to judge the general quality of our results. The only way was to compare our experiments with results from the recent fluid dynamics literature, as well as with the rare observations of natural events, where exit velocities, column height, and mass flow rate were measured (e.g. the eruption of Montserrat volcano, Formenti et al. (2003)).

Our experiments show that in the case of dense collapsing columns forming pyroclastic density currents, the entrainment of external fluid is not significant, which is in agreement with the results of the analytical and numerical calculations presented here. Similar conclusions were reached by other authors by means of observation of natural events (Formenti et al. 2003) and of theoretical considerations (Carazzo et al. 2008). This outcome agrees well with the recent fluid dynamics literature, where it is suggested that with Fr_0' smaller than

3, entrainment is not effective (Kaye and Hunt 2006; Lin and Armfield 2008). The same result was obtained by our experiments, and we suggest that this value of Fr_0' discriminates the source conditions leading to fallout vs. pyroclastic density currents. The cause of the lack of air entrainment is to be attributed to the large density difference at the interface between the internal and external fluid, as suggested by Kaminski et al. (2005), and not to the lack of turbulence, since our experiments are all at high Reynolds numbers. In the case of our cold dilute columns, the entrainment coefficient is about 0.06, which is similar to those of pure jets reported in the fluid dynamics literature (Turner 1986; Kaye and Hunt 2006; Carazzo et al. 2008). In contrast, for hot dilute columns driven by thermal buoyancy, the entrainment coefficient is about 0.11, which is similar to those of plumes (Turner 1986; Woods 2010). Both cold and hot dilute columns have densimetric Froude numbers greater than 3 and were successfully simulated by the numerical code, confirming the compatibility of our experimental measurements with a top-hat model. We note that even when there is no thermal buoyancy, and the Froude number is greater than 3, air entrainment produces a strong dilution of the gas-particle mixture, resulting in particle fallout from the column margin, but not in a collapse. We conclude that the only way to produce substantial density currents is by dense eruptive columns with no entrainment, which leads to densimetric Froude numbers lower than 3. Based on this outcome, it is possible to construct a diagram in which the source conditions (exit velocity, conduit radius, and particle volumetric concentration) define the stability fields of pyroclastic density currents vs. fallout. Such a stability field diagram is shown in Fig. 11, where the threshold limit of 3 for the densimetric Froude number is used to draw the solid curves delimiting the field of pyroclastic flows (areas under the curves) vs. pyroclastic fallout (areas above the curves), as a function of exit velocity and conduit radius. The solid curves represent particle volumetric concentrations (and the corresponding values of gas mass fraction) at the vent, and the dashed curves represent the total mass flow rate. The diagram agrees well with a similar diagram proposed by Dellino et al. (2010), which uses as a threshold limit the value of 500 s^{-1} for the vorticity factor Ω, which discriminates convective plumes (when $\Omega > 500$ s^{-1}) from collapsing columns (when $\Omega < 500$ s^{-1}), and is given by

$$\Omega = \frac{2U_0}{r_0 C_0} \qquad (21)$$

This means that the vorticity factor discriminates the eruptive regime in a similar way as the initial densimetric Froude number, which is not surprising since vorticity controls the ability of the gas-particle flow to mix with the surrounding fluid.
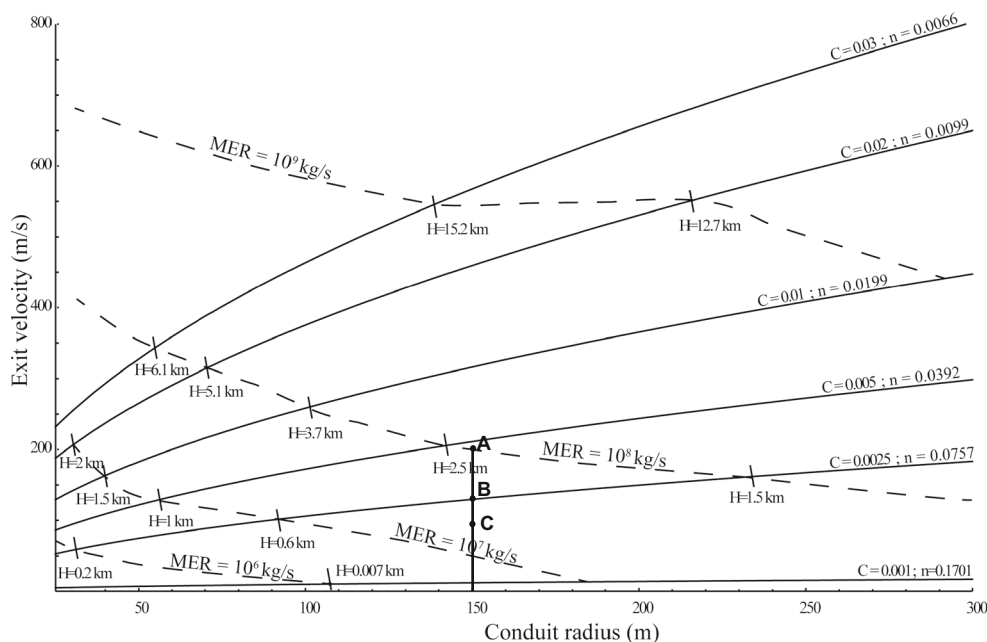
Fig. 11 Diagram based on the threshold value $Fr_0' = 3$, showing the stability field of pyroclastic fallout vs. pyroclastic density current as a function of conduit radius and exit velocity. The *solid lines* represent various values of particle volumetric concentration, C, and corresponding gas mass fraction, n. For the given C and n, the area below each curve is the stability field of pyroclastic density currents. The area above the curve is the stability field of pyroclastic fallout. The *dashed lines* represent various values of mass eruption rate, MER. The value of the height from which the column collapses in the natural case, H, based on the Bernoulli's equation, is shown at the intersections of the *dashed lines* and *solid lines*. Points A, B, and C lying on the line $r = 150$ m are added for comparison with the stability fields proposed by Degruyter and Bonadonna (2013)

Previous studies have shown that larger conduit radii and lower exit velocities favor collapsing columns and lead to the formation of pyroclastic density currents, as do lower gas mass fractions (higher particle volumetric concentrations). Figure 11 also shows this general behavior, but when we compare it in detail with similar diagrams of the literature, significant differences emerge regarding the values at which the transition between the two eruptive styles occurs. The stability field of collapsing columns is quite different, for example, from that of Wilson et al. (1980) (see also Cioni et al. 2000). The agreement is relatively good only for rather high particle volumetric concentrations ($C_0 = 0.0133$; low gas mass fractions, $n_0 = 0.01$), while for lower particle concentrations (higher gas mass fractions), and a given conduit radius, the limit between convective plumes and collapsing columns is met at higher exit velocities than in Wilson et al. (1980). This means that the stability field of collapsing columns calculated by our model is wider. This is likely due to the fact that the Wilson et al. (1980) diagram was calculated based on Morton's plume theory, which should not be applied to dense collapsing columns, as emphasized by Carazzo et al. (2008). Indeed, dense columns violate the assumptions of Morton's model, specifically the one that states that scalar quantities (in our case solid particles) must not significantly change the density of the fluid (assumption (4)). Our diagram agrees reasonably well with that proposed by Carazzo et al. (2008) if the combination of exit velocity and particle volumetric concentration is set to define the total mass flow rate. The Carazzo et al. (2008) diagram results, as does ours, from a model based on a variable entrainment coefficient that is quite low for small gas mass fractions. Furthermore, good agreement is observed between Fig. 11 and the regime diagrams proposed by Suzuki and Koyaguchi (2012). In particular, we have compared results on the transition between the fountain-type collapse and the other regimes by extracting from the curve the exit velocity that corresponds to a fixed mass eruption rate (MER) value. Our exit velocities at the transition (for the corresponding gas mass fraction n) agree reasonably well with those of Suzuki and Koyaguchi (2012), and the observed scatter (about 20–40 m s^{-1}) can probably be attributed to the lack of conduit radius value in their diagram. In order to further constrain the similarity between the two diagrams, we calculated the Fr_0' from the simulations of Suzuki and Koyaguchi (2012) for fountain-type collapses and verified that the Froude number is always below our proposed threshold limit of 3, thus well within the collapsing column regime. Finally, we compared our diagram with the regime diagrams of Degruyter and Bonadonna (2013) upon calculating, for some selected points shown in Fig. 11, their Γ_1 parameter (Eq. 20). Degruyter and Bonadonna (2013) also consider a second parameter, which is dependent on wind entrainment; in our calculations, the effect of wind was neglected, thus this parameter is set to 0. Point A in Fig. 11 ($U_0 = 200$ m s^{-1}, $r = 150$ m) falls in the buoyant plume stability

field above the curve $C=0.025$, which we choose here as a representative value. If the entrainment coefficient is taken equal to 0.1 (which is reasonable for a buoyant plume) a value of $\Gamma_1=1.12$ is found for this point, which is well within the buoyant plume stability field in the diagram of Degruyter and Bonadonna (2013). For point B ($U_0=130$ m s^{-1}, $r=150$ m) lying on the transition curve $C=0.025$, if the entrainment coefficient is taken equal to 0.05 (close to the condition leading to collapsing columns), a value of $\Gamma_1=5.3$ is found, which lies in the transition field of Degruyter and Bonadonna's diagram. Finally, for point C ($U_0=90$ m s^{-1}, $r=150$ m), which falls in the collapsing column stability field below the transition curve $C=0.025$, if the entrainment coefficient is taken equal to 0.05, a value of $\Gamma_1=11.1$, well within the collapse field of Degruyter and Bonadonna (2013) is found. These three examples show that our stability field diagram and the one by Degruyter and Bonadonna (2013), which are based on different data and theoretical considerations, give similar results that help in the interpretation of explosive eruption regimes by means of fluid dynamics scaling laws.

The height at which collapse occurs, H, as calculated by Bernoulli's equation (Eq. 15), is marked on the various curves in Fig. 11. This collapse height is much less than that proposed by Woods (1988). The difference is due to the fact that in Woods (1988), collapsing columns are calculated on the assumption that even when buoyancy is not achieved, an entrainment coefficient of 0.06 is maintained, which can cause a collapse. However, this is not the case in our experiments and numerical simulations, which suggest instead that column collapse (and formation of significant density currents) is obtained only in the case of no entrainment.

The use of Fig. 11 can help to constrain the initial conditions and eruptive style (pyroclastic flow vs. fallout) of hazardous explosive volcanoes. For example, if field data of pyroclastic flow deposits are used to constrain conduit radius or mass eruption rate (when the total volume of pyroclastic deposits is known, and eruption duration can be assumed), it is possible to set the threshold limit ($Fr_0'=3$) for the formation of a collapsing column, calculate the exit velocity, and find the approximate value of maximum height by means of Bernoulli's equation. This would set a fundamental constraint on the potential energy for the collapse, which ultimately controls the runout of a pyroclastic density current. The verification of this hypothesis, and its consequences for the mobility and potential impact of ensuing pyroclastic flows, represent the future development of this research. This analysis will be carried out with theoretical and numerical models that will be validated experimentally and verified by field data. Another possible step towards a better understanding of column dynamics would be to compare the video footage of our experimental columns with those of real eruptions, in order to apply the video analysis proposed here and compare results with previous analysis (e.g., Andrews and Gardner 2009).

References

Andrews B, Gardner J (2009) Turbulent dynamics of the 18 May 1980 Mount St. Helens eruption column. Geology 37(10):895–898. doi:10.1130/G30168A.1

Bloomfield LJ, Kerr RC (2000) A theoretical model of a turbulent fountain. J Fluid Mech 424:197–216. doi:10.1017/S0022112000001907

Carazzo G, Kaminski E, Tait S (2006) The route to self-similarity in turbulent jets and plumes. J Fluid Mech 547:137–148. doi:10.1017/S002211200500683X

Carazzo G, Kaminski E, Tait S (2008) On the dynamics of volcanic columns: a comparison of field data with a new model of negatively buoyant jets. J Volcanol Geotherm Res 178:94–103. doi:10.1016/j.jvolgeores.2008.01.002

Carazzo G, Kaminski E, Tait S (2010) The rise and fall of turbulent fountains: a new model for improved quantitative predictions. J Fluid Mech 657:265–284. doi:10.1017/S002211201000145X

Cioni R, Marianelli P, Santacroce R, Sbrana A (2000) Plinian and subplinian eruptions. In: Sigurdsson H (ed) Encyclopedia of volcanoes. Academic, New York, pp 477–494

Costa A, Macedonio G, Folch A (2006) A three-dimensional Eulerian model for transport and deposition of volcanic ashes. Earth Planet Sci Lett 241:634–647. doi:10.1016/j.epsl.2005.11.010

Degruyter W, Bonadonna C (2013) Impact of wind on the condition for column collapse of volcanic plumes. Earth Planet Sci Lett 377–378:218–226. doi:10.1016/j.epsl.2013.06.041

Dellino P, Zimanowski B, Büttner R, La Volpe L, Mele D, Sulpizio R (2007) Large-scale experiments on the mechanics of pyroclastic flows: design, engineering, and first results. J Geophys Res 112, B04202. doi:10.1029/2006JB004313

Dellino P, Dioguardi F, Zimanowski B, Büttner R, Mele D, La Volpe L, Sulpizio R, Doronzo DM, Sonder I, Bonasia R, Calvari S, Marotta E (2010) Conduit flow experiments help constraining the regime of explosive eruptions. J Geophys Res 115, B04204. doi:10.1029/2009JB006781

Dioguardi F, Dellino P, de Lorenzo S (2013) Integration of large-scale experiments and numerical simulations for the calibration of friction laws in volcanic conduit flows. J Volcanol Geotherm Res 250:75–90. doi:10.1016/j.jvolgeores.2012.09.011

Fischer HB, List EJ, Koh RCY, Imberger J, Brooks NH (1979) Mixing in inland and coastal waters. Academic, New York

Formenti Y, Druitt TH, Kelfoun K (2003) Characterization of the 1997 Vulcanian explosions of Soufrière Hills Volcano, Montserrat, by video analysis. Bull Volcanol 65:587–605. doi:10.1007/s00445-003-0288-8

Isaia R, D'Antonio M, Dell'Erba F, Di Vito M, Orsi G (2004) The Astroni volcano: the only example of closely spaced eruptions in the same vent area during the recent history of the Campi Flegrei caldera (Italy). J Volcanol Geotherm Res 133:171–192. doi:10.1016/S0377-0273(03)00397-4

Kaminski E, Tait S, Carazzo G (2005) Turbulent entrainment in jets with arbitrary buoyancy. J Fluid Mech 526:361–376. doi:10.1017/S0022112004003209

Kaye NB, Hunt GR (2006) Weak fountains. J Fluid Mech 558:319–328. doi:10.1017/S0022112006000383

Koyaguchi T, Woods AW (1996) On the formation of eruption columns and pyroclastic flow generations. J Geophys Res 101(B3):5561–5574

Koyaguchi T, Suzuki YJ, Kozono T (2010) Effects of the crater on eruption column dynamics. J Geophys Res 115, B07205. doi:10.1029/2009JB007146

Lin W, Armfield SW (2000) Direct simulation of weak axisymmetric fountains in a homogeneous fluid. J Fluid Mech 403:67–88. doi:10.1017/S0022112099006953

Lin W, Armfield SW (2008) Onset of entrainment in transitional round fountains. Int J Heat Mass Transfer 51:5226–5237. doi:10.1016/j.ijheatmasstransfer.2008.02.047

McDougall TJ (1981) Negatively buoyant vertical jets. Tellus 33:313–320

Mele D, Sulpizio R, Dellino P, La Volpe L (2011) Stratigraphy and eruptive dynamics of a pulsating Plinian eruption of Somma-Vesuvius: the Pomici di Mercato (8900 years B.P.). J Volcanol Geotherm Res 73:257–278. doi:10.1007/s00445-010-0407-2

Morton BR, Taylor GI, Turner JS (1956) Turbulent gravitational convection from maintained and instantaneous source. Proc R Soc Lond 234:1–23

Ogden DE, Glatzmeier GA, Wohletz KH (2008) Effects of vent overpressure on buoyant eruption columns: implications for plume stability. Earth Planet Sci Lett 268:283–292. doi:10.1016/j.epsl.2008.01.014

Papanicolaou PN, List EJ (1988) Investigations of round vertical turbulent buoyant jets. J Fluid Mech 195:341–391. doi:10.1017/S0022112088002447

Papanicolaou PN, Papakonstantis IG, Christodoulou GC (2008) On the entrainment coefficient in negatively buoyant jets. J Fluid Mech 614:447–470. doi:10.1017/S0022112008003509

Press WH, Teukolsky SA, Vetterling WT, Flannery BP (1996) Numerical recipes in Fortran 90. The art of parallel scientific computing, 2nd edn. Cambridge University Press, Cambridge

Saffaraval F, Solovitz SA, Ogden DE, Mastin LG (2012) Impact of reduced near-field entrainment of overpressured volcanic jets on plume development. J Geophys Res 117, B05209. doi:10.1029/2011JB008862

Sparks RSI, Bursik MI, Carey SN, Gilbert JS, Glaze LS, Sigurdsson H, Woods AW (1997) Volcanic plumes. Wiley, New York

Sulpizio R, Folch A, Costa A, Scaini C, Dellino P (2012) Hazard assessment of far-range volcanic ash dispersal from a violent Strombolian eruption at Somma-Vesuvius volcano, Naples, Italy: implications on civil aviation. Bull Volcanol 74:2205–2218. doi:10.1007/s00445-012-0656-3

Suzuki YJ, Koyaguchi T (2009) A three-dimensional numerical simulation of spreading umbrella clouds. J Geophys Res 114, B03209. doi:10.1029/2007JB005369

Suzuki YJ, Koyaguchi T (2012) 3-D numerical simulations of eruption column collapse: effects of vent size on pressure-balanced jet/plumes. J Volcanol Geotherm Res 221–222:1–12. doi:10.1016/j.jvolgeores.2012.01.013

Suzuki YJ, Koyaguchi T, Ogawa M, Hachisu I (2005) A numerical study of turbulent mixing in eruption clouds using a three-dimensional fluid dynamics model. J Geophys Res 110, B08201. doi:10.1029/2004JB003460

Turner JS (1966) Jets and plumes with negative or reversing buoyancy. J Fluid Mech 26:779–792. doi:10.1017/S0022112066001526

Turner JS (1986) Turbulent entrainment: the development of the entrainment assumption, and its application to geophysical flows. J Fluid Mech 173:431–471. doi:10.1017/S0022112086001222

Wilson L (1976) Explosive volcanic eruptions—III. Plinian eruption columns. Geophys J R Astron Soc 45:543–556

Wilson L, Sparks RSJ, Walker GPL (1980) Explosive volcanic eruptions—IV. The control of magma properties and conduit geometry on eruption column behavior. Geophys J R Astron Soc 63:117–148

Woods AW (1988) The fluid dynamics and thermodynamics of eruption columns. Bull Volcanol 50:169–193. doi:10.1007/BF01079681

Woods AW (1993) Moist convection and the injection of volcanic ash into the atmosphere. J Geophys Res 98:17627–17636. doi:10.1029/93JB00718

Woods AW (2010) Turbulent plumes in nature. Annu Rev Fluid Mech 43:391–412. doi:10.1146/annurev-fluid-121108-145430

Woods AW, Bursik M (1991) Particle fallout, thermal disequilibrium and volcanic plumes. Bull Volcanol 53:559–570. doi:10.1007/BF00298156

Woods AW, Caulfield CP (1992) A laboratory study of explosive volcanic eruptions. J Geophys Res 97:6699–6712. doi:10.1029/92JB00176